Decomposition-based Multiscale Compressed Sensing

Thuong Nguyen Canh[1], Khanh Quoc Dinh[2], and Byeungwoo Jeon[3]
College of Information and Computer Engineering, Sungkyunkwan University, Suwon, Korea
{[1]ngcthuong, [3]bjeon}@skku.edu

***Abstract*— This paper proposes a generalized decomposition-based measurement matrix (DMM) to capture multi-scale compressive measurements. In the proposed method, we linearly decompose the sensing image to various scales, and then adaptively sample it at each scale to capture essential information. The restricted isometric property of DMM is proven for structured sparse and compressible signals with various decomposition methods. Simulation results validate the recovery performance of the proposed method as well as the reduction in complexity.**

***Keywords*— Compressive sensing, sparse matrix, multiscale**

I. INTRODUCTION

Compressive sensing (CS) [1, 13] is a well-known modern sampling technique capable of recovering high-resolution signals from under-sampled data. Researchers often use the Gaussian random matrix (GRM) as a sensing matrix due to its theoretical performance [1]. Because of its fully random nature, GRM poses practical difficulties such as requiring significant resources in storage and computation especially for high dimensional signals like image and video. To lessen this complexity, a block-based version (BCS) [2, 16] and a separable version with Kronecker product (KCS) [3] were proposed.

While CS utilizes only sparsity prior in general, image/video signals, however, are well-known to have low-frequency prior (i.e., human visual system is more sensitive at low-frequencies than high-frequencies [7, 8]). We further note that CS was extended to hybrid [4, 15] and multi-scale [2, 4, 6, 17] schemes to favor the low-frequency parts, which brings significant improvement in sampling efficiency.

Image decomposition [7, 8] (e.g., multi-resolution, scale space, and pyramid, etc.) is a technique to split a signal to various scales with different amount of information. Decomposition has been widely used to analyze image characteristic in many applications like denoising, classification, segmentation, etc. CS utilizes decomposition for reconstruction [5, 12] and multi-scale sampling schemes [2, 6, 11, 17].

This paper attempts to generalize multi-scale sampling scheme with a decomposition-based measurement matrix (DMM). The proposed DMM achieves higher sampling efficiency and less storage requirement.

This research was supported in part by the National Research Foundation of Korea (NRF) grant (2017R1A2B2006518) funded by the Ministry of Science and ICT.
[2]He is now with Digital Media & Communications R&D Center, Samsung Electronics, Seoul, Korea

978-1-5386-2615-3/18/$31.00 ©2018 IEEE

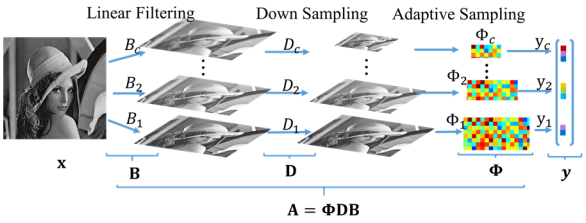

Fig. 1. Proposed Decomposition-based Measurement Matrix (DMM)

Our contributions in this paper are three-fold: (i) we propose a generalized multi-scale sensing matrix, (ii) we derive its RIP conditions for structured sparse and compressible signals with various decomposition methods, (iii) and we evaluate its performance with respect to various key factors and compare it to state-of-the-art sampling schemes.

The structure of this paper is as following. We briefly present general image decomposition in Section II. DMM matrices and theirs RIP condition are given in Section III. Section IV shows experimental results and conclusion is drawn in Section V.

II. GENERALIZED LINEAR IMAGE DECOMPOSITION

Generally, we can classify decomposition methods into linear (scale space, multi-resolution, pyramid decomposition, etc.) and non-linear (cartoon texture decomposition, etc.) ones. Linear image decomposition methods execute the linear projection sampling of CS. A natural image $x \in \mathbb{R}^n$ can be linearly decomposed into c layers, $\{x_l\}_{l=1}^{c}$, as,

$$x_l = D_l B_l x, \qquad l = 1, \cdots, c \tag{1}$$

where D_l denotes a down sampling matrix, and B_l a filter matrix. From Eq. (1), one can deliver various linear decompositions. For pyramid decomposition [8], each scale is obtained by blurring followed by down-sampling which corresponds to using B_l with a Gaussian kernel. The scale space and multi-resolution [7] decomposition can be obtained by setting D_l and B_l to an identity matrix, respectively. Wavelet decomposition also can be delivered by using high pass and low-pass linear filter B_l.

III. PROPOSED DECOMPOSITION-BASED SENSING

A. Decomposition-based Measurement Matrix (DMM)

As signal information varies across decomposed images, we would like to capture signal efficiently with an adaptive sensing scheme. As illustrated in Fig. 1, we first linearly decompose

input image into various scales, then adaptively sample (i.e., with adaptive number of measurements) at each scale with its sampling matrix. This process is equivalent to sampling with the proposed DMM matrix in Definition 1.

Definition 1: *Given set of the sensing, down-sampling, and blurring matrix matrices,* $\{\Phi_l\}_{l=1}^{c}, \{B_l\}_{l=1}^{c}, \{D_l\}_{l=1}^{c}$ *satisfy*

$$\Phi_l \in \mathbb{R}^{m_l \times n_l}, D_l \in \mathbb{R}^{n_l \times n}, B_l \in \mathbb{R}^{n \times n}, \tag{2}$$

where $m = \sum_{l=1}^{c} m_l$, *both* D_l *and* B_l *are circulant matrices, the decomposition-based multi-scale measurement matrix (named as DMM),* $A \in \mathbb{R}^{m \times n}$, *is constructed as*

$$A = [A_1; \dots; A_c] = [\Phi_1 D_1 B_1; \dots; \Phi_c D_c B_c], \tag{3}$$

B. The RIP condition of DMM

In this work, we present the generalized proof for various decomposition schemes for structured sparse and compressible signal. Note that, the characteristic of Φ_l, D_l, B_l has effect on the RIP condition of DMM with respect to decomposition method. Therefore, other assumption can be added for a corresponding decomposition method. Our proof is given as follows.

Assumption 1: *k-sparse signals* $\alpha \in \mathbb{R}^n$ *can be linearly decomposed to* c k_l*-sparse signals* $\alpha_l = D_l B_l \alpha \in \mathbb{R}^{n_l}$.

Assumption 2: *Each matrix* Φ_l *satisfies the RIP condition*

$$(1 - \delta_l)\|z\|_2^2 \le \|\Phi_l z\|_2^2 \le (1 + \delta_l)\|z\|_2^2, \tag{4}$$

for all $k_* = \max k_l$ *sparse signals,* $z \in \mathbb{R}^{n_k}$ *with a restricted isometry constant* δ_l.

Since Φ_l satisfies RIP condition for k_*, it also satisfies the RIP condition for all $k_l \le k_*$ sparse signals of dimension n_l.

From Assumptions 1 and 2, and $\Phi_l \alpha_l = A_l \alpha$, the inequality for each decomposed signal becomes

$$(1 - \delta_l)\|\alpha_l\|_2^2 \le \|A_l \alpha\|_2^2 \le (1 + \delta_l)\|\alpha_l\|_2^2. \tag{5}$$

Because of $\Phi_l \alpha_l = A_l \alpha$, by summing (5) for all l, we obtain

$$\sum_{l=1}^{c}(1 - \delta_l)\|\alpha_l\|_2^2 \le \sum_{l=1}^{c}\|A_l \alpha\|_2^2 \le \sum_{l=1}^{c}(1 + \delta_l)\|\alpha_l\|_2^2. \tag{6}$$

Let $\delta_* = \max\{\delta_l\}$, we can rewrite the inequality (6) as

$$(1 - \delta_*)\sum_{k=1}^{c}\|\alpha_l\|_2^2 \le \|A\alpha\|_2^2 \le (1 + \delta_*)\sum_{k}^{c}\|\alpha_l\|_2^2. \tag{7}$$

Now we prove RIP condition for various decomposition method.

1) DMM with Wavelet Decomposition (DMM-W)

It should be noted that, if a decomposed signal satisfies

$$\sum_{k=1}^{c}\|\alpha_k\|_2^2 = \|\alpha\|_2^2, \tag{8}$$

then, DMM is said to satisfy the RIP condition

$$(1 - \delta_*)\|\alpha\|_2^2 \le \|A\alpha\|_2^2 \le (1 + \delta_*)\|\alpha\|, \tag{9}$$

for a k-sparse signal α that satisfies Assumption 1 with an isometry constant δ_*. According to Parseval theorem of wavelet, DMM-W satisfies Eq. (9), thus guarantees the RIP condition for sparse signals which satisfy Assumption 1.

2) DMM with Scale Space (DMM-SS)

In this case, D_l is reduced to an identity matrix and we give an additional assumption for B.

Assumption 3. *Filter matrix* $B_l \in \mathbb{R}^{n \times n}$ *is a circulant matrix constructed from a normalized seed vector* $b_l \in \mathbb{R}^s$

$$\sum_{i=1}^{s} b_l^i = 1, b_l^i > 0, \ s \ll n. \tag{10}$$

The pth element of α_l is calculated as $\alpha_l^p = \sum_{i=1}^{s} b_l^i \alpha^{p+i-1}$. At a special case of index $p + i - 1 > n$, the value α^{p+i-1} becomes $\alpha^{p+i-1-n}$ as the circulant matrix B_l. We have the norm

$$\|\alpha_l\|_2^2 = \sum_{p=1}^{n}\left(\alpha_l^p\right)^2 = \sum_{p=1}^{n}\left(\sum_{i=1}^{s} b_l^i \alpha^{p+i-1}\right)^2 \tag{11}$$

$$= \underbrace{\sum_{p=1}^{n}\left(\sum_{i=1}^{s}\left(b_l^i \alpha^{p+i-1}\right)^2\right)}_{F_1} + \underbrace{2\sum_{p=1}^{n}\left(\sum_{i=1}^{s}\sum_{j\ne i}^{j\in\{1\cdots s\}} b_l^i b_l^j \alpha^{p+i-1}\alpha^{p+j-1}\right)}_{F_2}$$

As B_l is a circulant matrix of size $n \times n$, each scalar b_l^i is multiplied to all elements $\alpha^{j\prime}s$. Therefore, we have

$$F_1 = \sum_{i=1}^{s}\left(b_l^i\right)^2\left(\sum_{p=1}^{n}(\alpha^p)^2\right) = \|\alpha\|_2^2\sum_{i=1}^{s}\left(b_l^i\right)^2. \tag{12}$$

From the non-zero condition of filter kernel $b_k^i b_k^p > 0$ and

$$2\left|\alpha^{p+i-1}\alpha^{p+j-1}\right| \le \left(\alpha^{p+i-1}\right)^2 + \left(\alpha^{p+j-1}\right)^2, \tag{13}$$

leads to the inequality

$$F_2 \le \sum_{i=1}^{s}\sum_{j\ne i}^{j\in\{1,\dots,s\}} b_l^i b_l^j\left(\sum_{p=1}^{n}\left(\left(\alpha^{p+i-1}\right)^2 + \left(\alpha^{p+j-1}\right)^2\right)\right)$$

$$\Leftrightarrow F_2 \le 2\|\alpha\|_2^2\sum_{i=1}^{s}\sum_{j\ne i}^{j\in\{1,\dots,s\}} b_l^i b_l^j. \tag{14}$$

Thus, we can get the upper bound of $\|\alpha_l\|_2^2$ as

$$\|\alpha_l\|_2^2 \le \|\alpha\|_2^2\left(\sum_{i=1}^{s}(b_l^i)^2 + 2\sum_{i=1}^{s}\sum_{j\ne i}^{j\in\{1,\dots,s\}} b_l^i b_l^p\right) \tag{15}$$

$$\Leftrightarrow \|\alpha_l\|_2^2 \le \|\alpha\|_2^2\left(\sum_{i=1}^{s} b_l^i\right)^2 = \|\alpha\|_2^2. \tag{16}$$

On the other hand, the lower bound can be delivered as

$$\|\alpha_l\|_2^2 \ge \|\alpha\|_2^2\underbrace{\left(\sum_{i=1}^{s}\left(b_l^i\right)^2 - 2\sum_{i=1}^{s}\sum_{j\ne i}^{p\in\{1,\cdots,c\}} b_l^i b_l^j\right)}_{q\ge 0}. \tag{17}$$

From this inequality, DMM-SS satisfies the RIP condition of

$$q(1 - \delta_*)\|\alpha\|_2^2 \le \|A\alpha\|_2^2 \le (1 + \delta_*)\|\alpha\|_2^2. \tag{18}$$

for all k-sparse signals α that satisfy Assumption 1 with the restricted isometry constant of δ_*. Other cases of DMM-MR and DMM-PR are also easy to follow.

Table 1. Description of various sensing schemes

Algorithm	Descriptions
DTVNL[12]	Decomposition-based total variation, KCS
TVHyrbid[13]	Total variation with hybrid sensing (DCT & noiselet)
MH-MS [3]	Multi-scale BCS with multiple hypothesis, BCS
TGVSH[14]	TGV + Sheartlet, radial Fourier sensing
DMM-W [6]	DMM with Wavelet, DTVNL recovery, KCS
DMM-SS	DMM with Scale Space, DTVNL recovery, KCS
DMM-PR	DMM with PyRamid, DTVNL recovery, KCS

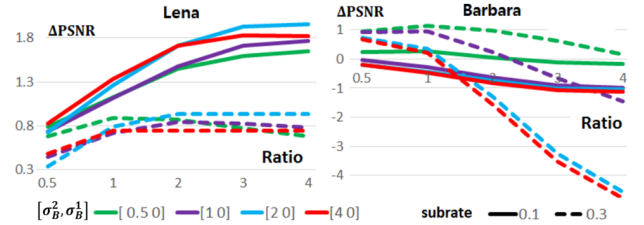

Fig. 2. ΔPSNR [dB] of DMM at decomposition 2 over GRM at various measurement ratios for Lena and Barbara.

C. *Discussion on the RIP condition of DMM*

The RIP condition of DMM is limited to signals satisfying Assumption 1 which is for structured sparse and compressible signal.

Sparse signal: It is easy to observe that the decomposed signal α_l can become less sparse (i.e., $k_l > k$) compared to α. The decomposed p-th value $\alpha_l^p = \sum_{i=1}^{s} b_l^i \alpha^{p+i-1}$ is more likely to be non-zero. In the worst case, α_l^p becomes a dense signal, so that δ_* will become very large, thus DMM does not satisfy RIP condition for all k-sparse signals.

Structured sparse signal. For structured sparse (for example, block sparse [9]) case, a decomposed signal α_l is less sparse compared to α. However, the worst case for α_l^p to become dense does not exist with sparse B, D matrices (i.e., $s << n$) as in Assumption 3. That is, if $\alpha^p \sim \alpha^{p+s}$ are zeros, its decomposed α_l^p is also zero. Thus, DMM satisfies RIP for structured sparse signal.

Compressible signal. A decomposed signal, by common decomposition methods like wavelet, is sparse in some selected domains. If we can approximate a compressible signal x as a k-sparse signal, then its decomposed one x_l is also can be approximated as a k_l sparse signal via k-term approximation [10]. Therefore, DMM satisfies RIP for compressed signals.

IV. Experimental Results

This section evaluates various factors of DMM and compares its performance with other state-of-the-art CS systems listed in Table 1 under the KCS framework. KCS requires two matrices $A^v, A^h \in \mathbb{R}^{\sqrt{m}\times\sqrt{n}}$ as

$$A = A^v \otimes A^h;\ Y = A^v X (A^h)^T,$$
$$\text{y} = vect(Y),\ \ x = vect(X), \tag{19}$$

where $vect(\cdot)$ denotes vectorization operator. X, Y are the 2D versions of 1D signals x, y, respectively. $(\cdot)^v, (\cdot)^h$ represent notations for horizontal and vertical directions, respectively. We use Gaussian i.i.d. matrix in KCS and simulate with test images

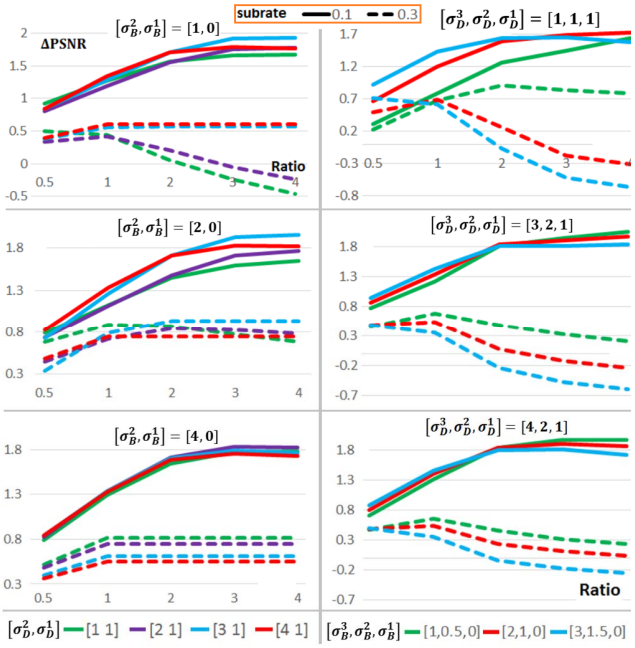

Fig. 3. ΔPSNR [dB] of DMM at decomposition 2 (1st), 3 (2nd column) over GRM for Lena images at various blurring levels.

of size 512 × 512 at subrates from 0.1 to 0.3 with averaging over five-times. Since each decomposition layer carries different amount of signal information, adaptive sampling scheme [2] is used to assign number of measurement for each layer.

For DMM-PR and DMM-SS, filter B_k is generated with a gaussian kernel with a standard deviation of σ_B^k. Note that $\sigma_B^k = 0$ means $B_k = I$ or no filtering. The down-sampling factor of D_k in DMM-PR and DMM-MR is represented as σ_D^k. For instance, $\sigma_D^k = 1$ means not-performing down-sampling and $\sigma_D^k = 2$ means performing down-sampling by factor of 2.

A. *Evaluation of Various Decomposition Methods*

The RIP condition of DMM depends on (i) the number of decomposition c, (ii) the down-sampling factor, (iii) number of assigned measurements (measurement allocation method), and (iv) the smoothness of filter. We evaluate the performance of the proposed sensing matrix through DMM-PR as it is a generalized version of DMM-SS and DMM-MR. DMM-W is measured by evaluating previous work [6]. We evaluate the proposed DMM-PR through decomposition level $c = 2$ as

$$A^i = \begin{bmatrix} A_1^i \\ A_2^i \end{bmatrix} = \begin{bmatrix} \Phi_1^i D_1^i B_1^i \\ \Phi_2^i D_2^i B_2^i \end{bmatrix} = \begin{bmatrix} \Phi_1^i \\ \Phi_2^i D_2^i B_2^i \end{bmatrix}, \tag{20}$$

where $D_1^i = B_1^i = I \in \mathbb{R}^{n\times n}$ and $i \in \{v, h\}$.

1) Measurement Allocation vs. Smoothing Filter

We vary the second filter B_2^i with various filter degrees, $\sigma_B^2 = [0.5, 1, 2, 4]$. Since we use a heuristic method [2] to allocate measurement for each layer $\{1, 2\}$, its heuristic parameter - the ratio seed is needed to evaluate. The experimental results in Fig. 3 show that, at a low subrate (r = 0.1), we should use higher scale or greater smoothness as it achieves the highest performance at ratio = 4. In contrast, DMM-

Table 3. Comparison of Performance in PSNR [dB] and SSIM

Image	Rate	DTVNL		MH-MS		TVHybrid		TGVSH		DMM-W		DMM-SS		DMM-PR	
		PSNR	SSIM	PSNR	SSIM	PSNR	SSIM	PSNR	SSIM	PSNR	SSIM	PSNR	SSIM	PSNR	SSIM
Lena	**0.1**	31.10	0.847	31.56	0.866	31.43	0.866	29.18	0.810	**32.87**	0.821	32.75	0.869	**33.15**	0.882
	0.2	34.44	0.901	34.95	0.916	34.33	0.915	34.22	0.902	**35.85**	0.919	**35.63**	0.912	35.61	0.913
	0.3	36.46	0.926	36.80	0.942	36.28	0.938	37.18	0.938	**37.67**	0.940	**37.30**	0.931	37.09	0.929
Barbara	**0.1**	25.15	0.715	24.25	0.637	24.15	0.701	24.30	0.706	24.89	0.725	**25.36**	0.715	**25.42**	0.719
	0.2	30.55	0.884	26.73	0.812	24.94	0.759	29.14	0.865	29.73	0.886	**31.81**	0.905	**31.77**	0.904
	0.3	33.88	0.933	28.17	0.873	25.99	0.821	33.10	0.934	33.15	0.938	**34.91**	0.943	**34.81**	0.942
Peppers	**0.1**	31.61	0.833	32.22	0.852	32.66	0.860	28.39	0.781	**33.20**	0.853	33.01	0.849	**32.20**	0.854
	0.2	34.25	0.876	34.77	0.987	34.81	0.892	33.79	0.866	**35.52**	0.891	34.98	0.879	**34.99**	0.882
	0.3	35.73	0.900	36.02	0.911	36.12	0.912	35.88	0.906	**36.59**	0.909	**35.98**	0.908	35.84	0.902
Camera-man	**0.1**	32.37	0.901	31.96	0.902	32.15	0.929	29.58	0.924	34.31	0.928	**34.31**	0.922	**34.89**	0.934
	0.2	36.19	0.945	38.12	0.963	36.29	0.971	36.31	0.975	38.72	0.967	**39.02**	0.966	**38.99**	0.969
	0.3	38.57	0.963	42.63	0.988	39.43	0.985	41.29	0.988	**41.79**	0.981	**42.03**	0.979	41.61	0.979
Average		33.36	0.885	33.19	0.890	32.38	0.879	32.69	0.883	34.52	0.897	34.76	0.898	**34.78**	**0.901**

Table 2. Storage requirement (in Mbytes) of an image of size n at subrate $r = 0.3$, decomposition level c, and q taps kernel for B, D.

Matrix	General		64x64		128x128	
	Rand	Cons	Rand	Cons	Rand	Cons
GRM	rn^2	0	36.3	0	581	0
DMM-SS	rn^2	cq	36.3	~0	581	~0
DMM-PR	γrn^2	$2cq$	12.2	~0	195	~0
DMM-W	γrn^2	$2q$	12.2	~0	195	~0

PR prefers to less smoothness with a filter degree $\sigma = 0.5$. It agrees with [11] that the measurement allocation should be signal-dependent as Barbara needs more samples at a fine scale.

2) Measurement Allocation vs. Down-sampling Factor

We evaluate the DMM performance at various scaling, $\sigma_D^2 = \{1, 2, 3, 4\}$ and blurring with $\sigma_B^2 = [1, 2, 4]$ for Lena image. As both down sampling D and smoothing B remove details in image, their impact on the final recovery performance is similar. The best allocation configuration is achieved at ratio = 4 for the low subrate and 0.5 for the high subrate. DMM-PR can reduce the complexity with almost similar performance to DMM-SS.

3) Memory Requirement for DMM

We compare the memory complexity of DMM at down sampling scales $\sigma_D = [\sigma_D^1, \dots, \sigma_D^c]$, the scalar value $\gamma = \sum_i^c \left(\left(\sigma_D^i\right)^{-1} \right)$. Table 2 shows that all DMM (excluding DMM-SS) significantly reduces the storage requirement compared to GRM thanks to the smaller size of their random matrices. Both DMM-PR, DMM-W show almost the same requirement.

B. Comparison with Other Sampling Schemes

We select the best setting for DMM-PR and DMM-SS at decomposition level 3. Table 3 shows that all DMM methods outperform the conventional KCS (DTVNL) [12] by 1.40 dB on average and up to 3.56 dB (Cameraman), surpassing TVHybrid [13] (2.39dB), TGVSH [14] (1.07dB) and MH-MS [2] (1.57 dB). All DMM methods produce very similar reconstruction performance. DMM-SS and PR offer better PSNR than DMM-W at low subrate and in images with rich structure (Barbara) or compressible (Cameraman). DMM-PR is more flexible in scaling factor than DMM-W (i.e. limited to the power of two).

V. Conclusions

In this paper we proposed a multi-scale measurement matrix based on image decomposition. We showed that it improves sampling efficiency as well as reduces complexity. Theoretical results and extensive experiments have validated better performance of DMM over GRM. The proposed method can be further extended to spatial scalable image/video application.

References

[1] D. L. Donoho, "Compressed sensing," IEEE Trans. Info. Theo., vol. 52, no. 4, pp. 1289–1306, Apr. 2006.

[2] J. Fowler et. al, "Multiscale block compressed sensing with smoothed projected Landweber reconstruction," in Sig. Process. Conf., Euro, pp. 564– 568, Aug. 2011.

[3] M. F. Duarte and R. G. Baraniuk, "Kronecker compressive Sensing," IEEE Trans. Image Process., vol. 21, no.2, pp. 494–504, Feb. 2012.

[4] Y. Tsaig and D. L. Donoho, "Extensions of compressed sensing," J. Sig. Process., vol. 86, no. 3, pp. 549–571, Mar. 2006.

[5] T. N. Canh et al, "Compressive sensing reconstruction via decompostion," Sig. Process. Image Comm., vol. 49, pp. 63-78, Nov. 2016.

[6] T. N. Canh et al, "Multiscale/multi-resolution Kronecker compressive imaging," in IEEE Inter. Conf. Image Process., pp. 2700–2704, 2015.

[7] Tony Lindeberg, Scale-space theory in computer vision, Kluwer, 1994.

[8] P. Burt and E. Adelson, "The laplacian pyramid as a compact image code," IEEE Trans. Comm., vol. 31, no. 4, pp. 532–540, Apr. 1983.

[9] Y. Eldar et al "Block-sparse signals: Uncertainty relations and efficient recovery," IEEE Trans. Sig. Process., vol.58, no.6, pp.3042–3054, 2010.

[10] A. Cohen, W. Dahmen and R. DeVore, "Compressed sensing and best k-term approximation," J. Amer. Math. Soc., vol 22, pp. 211-231, 2009.

[11] B. Roman, B. Adcock, and A. Hansen, On asymptotic structure in compressed sensing, Available at Arvix.org (arXiv: 1406.4178), 2014.

[12] T. N. Canh et al, "Detail preserving compressive sensing recovery based on cartoon texture image decomposition," in IEEE Inter. Conf. Image Process. (ICIP), pp. 1327–1331, Oct. 2014.

[13] J. Romberg, "Imaging via Compressive Sampling," IEEE Sig. Process. Mag., vol. 25, no. 2, pp. 14–20, Mar. 2008.

[14] W. Guo, J. Qin, and W. Yin, "A New Detail-Preserving Regularization Scheme," SIAM J. Imaging Sci., vol. 7, no. 2, pp. 1309–1334, Jan. 2014.

[15] T. N. Canh et al , "Hybrid Kronecker compressive sensing for images," in IEEE Int. Conf. on Advanced Tech. for Comm., pp. 1-5, Nov. 2014.

[16] K. Q. Dinh and B. Jeon, "Iterative Weighted Recovery for Block-based Compressive Sensing of Image/Video at Low Subrate," IEEE Trans. Cir. Sys. Video Tech., vol. 27, no.. 11, pp. 2294-2308, Nov. 2017.

[17] T. N. Canh et al, "Multi-Resolution Kronecker Compressive Sensing," IEIE Trans. Smart Process. Comput., vol.3, no.1, pp.19-27, Feb. 2014